Project Acronym:

MRBREASTBIO (CONCEPT/0521/0040)

MRI breast robotic system for biopsy

Deliverable number: 5.3

Title: Assessing the accuracy of the biopsy needle in reaching targets in the phantom.

Prepared by:

Anastasia Antoniou (CUT)
Christakis Damianou (CUT)
Anastasia Nikolaou (CUT)
George Lazarou (CUT)
Christos Yiallouras (MEDSONIC)

Date: 8/5/2023

Co-funded by the European Union

Republic of Cyprus

RESEARCH & INNOVATION FOUNDATION

Contents

Executive summary

The current deliverable presents the work carried out to assess the targeting accuracy of the biopsy needle. Phantoms mimicking breast tissue and tumour were utilized as the main tool for evaluating the developed biopsy robot in terms targeting accuracy, as well as the functionality of the biopsy software and integrated navigation algorithms.

The phantoms utilized in the study were made of agar gels simulating both breast tissue and embedded tumor mimics, which differed in the concentration of inclusions. The tumour mimics had a spherical shape and diameter ranging from 5 mm to 15 mm and served as the biopsy targets appearing as darker spots of reduced intensity on a brighter background in the MRI scans.

The needle positioning mechanism incorporates ultrasonic piezoelectric motors for motion actuation and optical encoders for motion feedback (deliverable 3.1), which were wired up to an electronic driving system located outside the MRI room through shielded cable. The custom-designed MRI-guided biopsy software (deliverable 3.3) allowed navigation planning on MRI images for manoeuvring the biopsy needle relative to the region of interest.

Two different methods were implemented for evaluating the needle targeting accuracy in the benchtop setting. In the first method, the needle was commanded to reach preselected tumour mimics and manually inserted in the phantom by the user. Needle navigation was based on MRI images. The success of the procedure was assessed visually by checking whether the plastic needle pierced the tumour at the desired location as commanded by the software. Tumours of different size (5-15 mm in diameter) were targeted multiple times (n=10) to check the system's repeatability. A laser-based approach was also followed, where a laser pointer was navigated to target random cells of a plastic grid. In this case, the needle positioning error was defined by the difference in the location of the red light and the targeted grid cell.

Phantom testing was then done in 1.5 T and 3T MRI scanners. The technique involved the use of a water-filled syringe, which was navigated to reach the location of a targeted tumour mimic (in an X-Y plane) as determined by the software coordinates. After navigation, Spin Echo (SE) images of the syringe and the phantom were overlapped to examine whether the new position of the syringe coincides with the tumour's location. After confirming proper positioning of the needle navigator, the syringe was replaced by a 3D printer plastic needle, which was manually inserted in the phantom to puncture the tumour. Again, the needle tip position relative to the tumour was visualized in T1-W and T2-Weighted (T2-W) images for assessing the targeting accuracy.

1. Introduction

All methodologies for testing a robot's mechanical accuracy and specifically the accuracy and repeatability of positioning a biopsy needle, are based on comparing the commanded with the actual motion step as determined by a distance-measuring technique. Before a process can be implemented in *in vivo* applications, its accuracy is typically assessed in free space, also known as the intrinsic system accuracy. Despite demonstrating appropriate motion accuracy and repeatability through benchtop testing, the system should be employed in the real environment (e.g., MRI) to ensure that a high level of accuracy is achieved.

Several motion tracking methods were employed in the context of evaluating the motion accuracy in benchtop experiments [1]–[6]. For needle interventions, optical tracking devices have been frequently utilized to validate acceptable targeting accuracy, where the placement error was defined as the divergence of the actual from the intended location of the needle tip [1]–[4]. As an example, a robot designed for breast biopsy was tested by navigating a rigid testing tool to reach target positions following both straight and curved pathways and tracking its motion using an optical tracker [1]. In another study by Groenhuis et al. [7], the accuracy of the needle tip of a breast biopsy robot was tested in free air utilizing a board with multiple crosshairs. The needle tip was instructed to puncture these targets, and the positioning error was calculated by measuring the distance between the center of each target and the respective punched hole [7].

High quality breast biopsy phantoms constitute a valuable tool in needle biopsy training and experimentation, as well as in testing the needle positioning accuracy of robotic-assisted biopsy devices. Commercially available breast biopsy phantoms are composed of patented realistic and durable breast tissue with several types of masses of varying sizes interspersed randomly throughout it. Membranes mimicking skin are utilized to cover the tissue proving realistic needle resistance to trainers [8]–[11].

Not only commercially available, but also “laboratory” phantoms have been proposed over time for biopsy training purposes. In fact, many institutions preferred “home-made” alternatives for their studies, utilizing food or animal products, since they are of lower-cost and easy to make. Turkey or chicken breast, as well as gel-based breast phantoms are commonly used to simulate soft tissue [12]. However, it seems that chicken and turkey breast are more realistic regarding mechanical properties [13]. The inserts could be of liquid or solid content depending on the type of biopsy procedure that will be followed. For freehand US-guided breast biopsy training, raw materials including olives with pimentos, capers, grapes, peas, potatoes, and strawberries have been proposed in the literature to mimic breast masses [12].

Household and raw materials were also selected for mimicking lesions in MR-compatible breast phantoms. In that case, the success of the procedure can be confirmed by visualization of the tumour material in the obtained sample [14], the void on follow up MRI [15], or the needle position relative to the target on intraoperative MRI. For instance, in one study [14], the reliability of an MR-guided biopsy procedure was tested in agarose phantoms containing peas, where the biopsy success was confirmed by visual inspection of the specimen. Schneider et al. [15] assessed a core biopsy system in a unique phantom, in which breast tissue was mimicked by a grapefruit and the tumour by an embedded long wooden dowel. The success of the procedure was defined by whether pieces of the wooden dowel were contained within the sample, as well as from the void showed up on follow up MRI [15]. Notably, the Gadopentetate dimeglumine (Gd-DTPA) contrast agent can be added in gel-based lesion mimics to improve the MRI contrast with respect to the surrounding breast-mimicking tissue [16]-[17].

The current study presents simple benchtop and MRI methods for testing the targeting accuracy of a biopsy needle in the framework of evaluating the developed MRI-guided robotic device for breast biopsy.

2. Benchtop evaluation

Repeatability test in phantoms with biopsy targets

Methodology

The purpose of this experiment was to assess both the accuracy and repeatability of robotic motion in dedicated biopsy phantoms. Two agar-based phantoms were developed by molding in specially designed molds (as described in the Deliverable 4.1). The first one contains 3 spherical biopsy targets of different size whereas the second one contains a cherry tomato. These phantoms are shown in **Figure 1**. The experimental setup as arranged in the laboratory setting with the phantom mounted on the dedicated holder of the robotic device is shown in **Figure 2.** The device was interfaced to the laptop with the relevant biopsy software through the custom made electronic driving system.

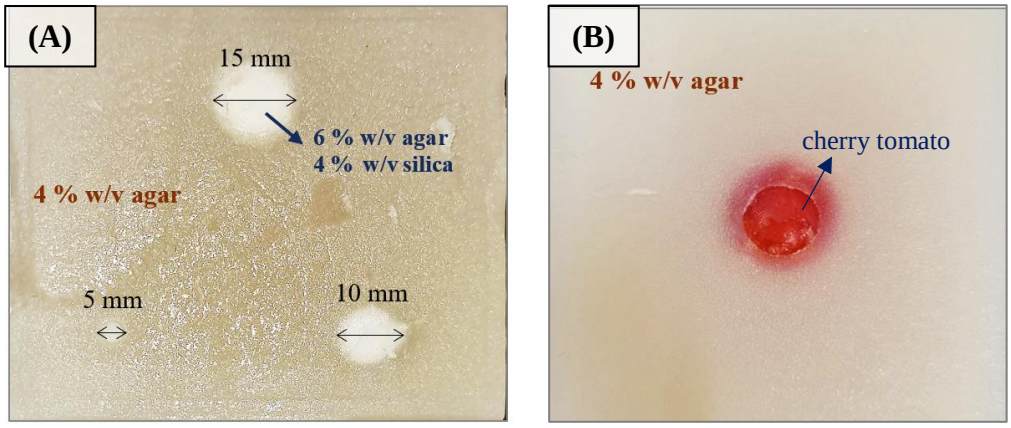

Figure 1*: (A) Agar-based phantom with biopsy targets of varying size (cross section). (B) Agar-based phantom containing a cherry tomato.*

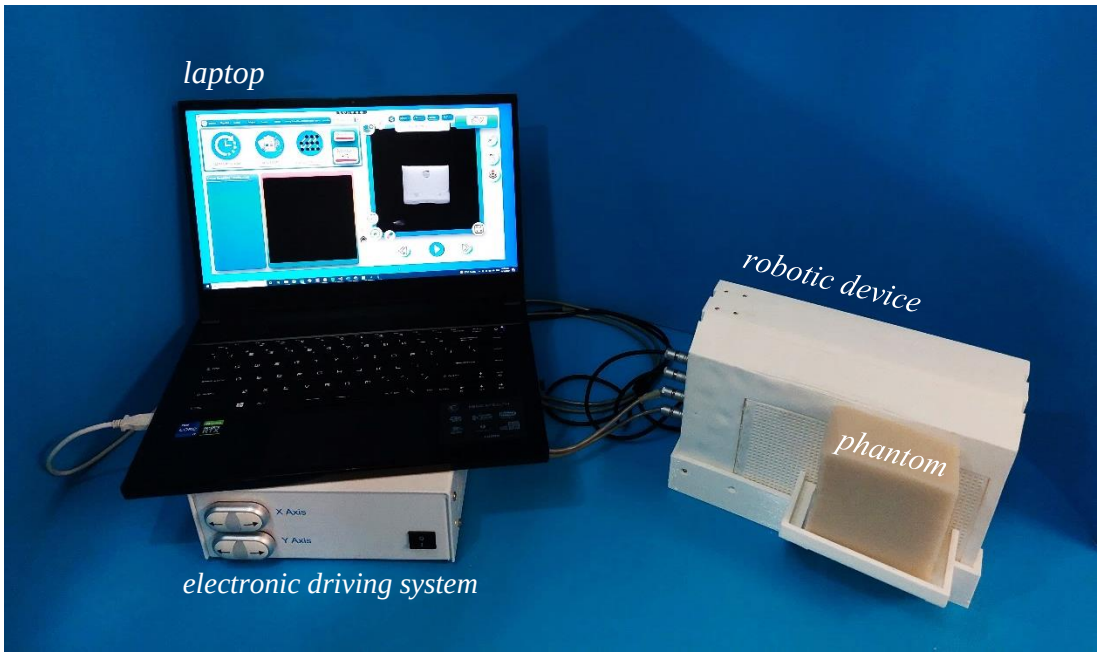

Figure 2*: Experimental setup for assessing the needle targeting accuracy in benchtop setting.*

In benchtop experiments, the biopsy software allowed navigation planning of the needle to the desired location based on previously obtained MRI images. Scans acquired at the level of the needle and phantom (involving the use of fiducial markers) were utilized, thus enabling needle registration relative to the targeted area (deliverable 3.3).

Accordingly, the user selected the target location on the relevant DICOM image showing the phantom and the extracted motion vectors defining the two-dimensional needle's path were sent to the electronic driving system for execution. Once the needle was placed at the location determined by the software coordinates (perpendicular to the grid), it was manually inserted in the phantom to puncture the target. All embedded tumour mimics were targeted one by one. The success of the procedure was assessed visually by checking whether the plastic needle pierced the tumour at the location defined by the software. Needle navigation to each tumour was performed 10 times to check the repeatability. **Figure 3** shows a screenshot of the software during navigation planning.

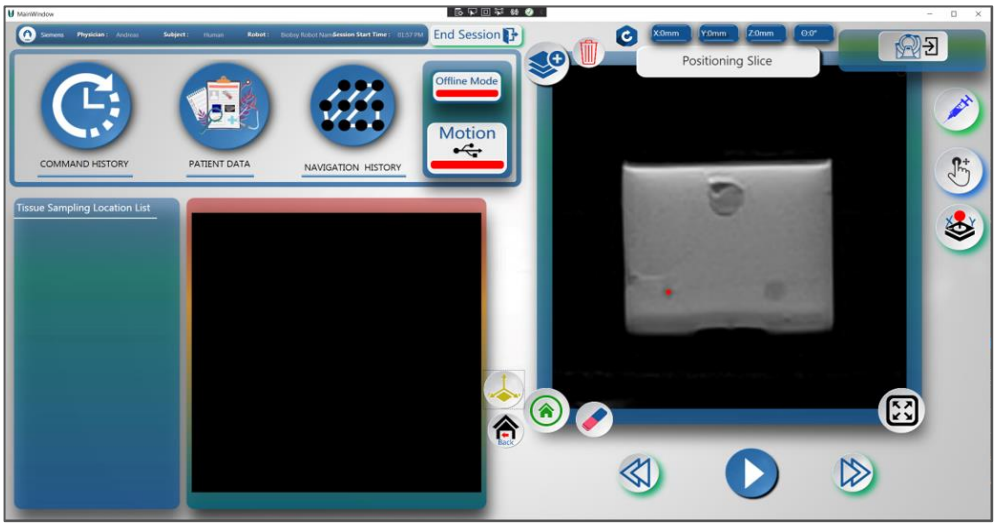

***Figure 3**: Screenshot of the software during navigation planning for the phantom study.*

Results

Figure 4 shows the target location as defined on the MRI image of the phantom containing a cherry tomato, whereas **Figure 5** shows photos of the phantom after motion execution and needle insertion for the 10 repetitions. The corresponding targeting results obtained for the 15- and 5- mm tumours of the multiple-tumour phantom are presented in **Figures 6-7** and **Figures 8-9**, respectively. In all the cases, the needle pierced the targeted tumour successfully. Furthermore, there is a very good agreement in the location of the needle tip among repetitions.

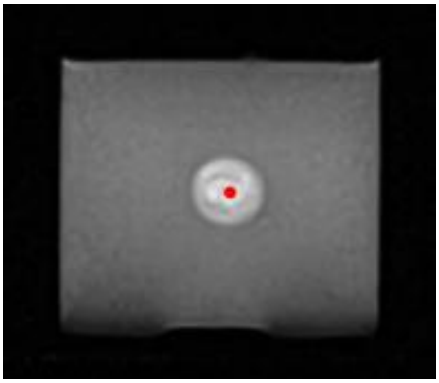

***Figure 4**: Target location as set on MRI image in the biopsy software (cherry tomato).*

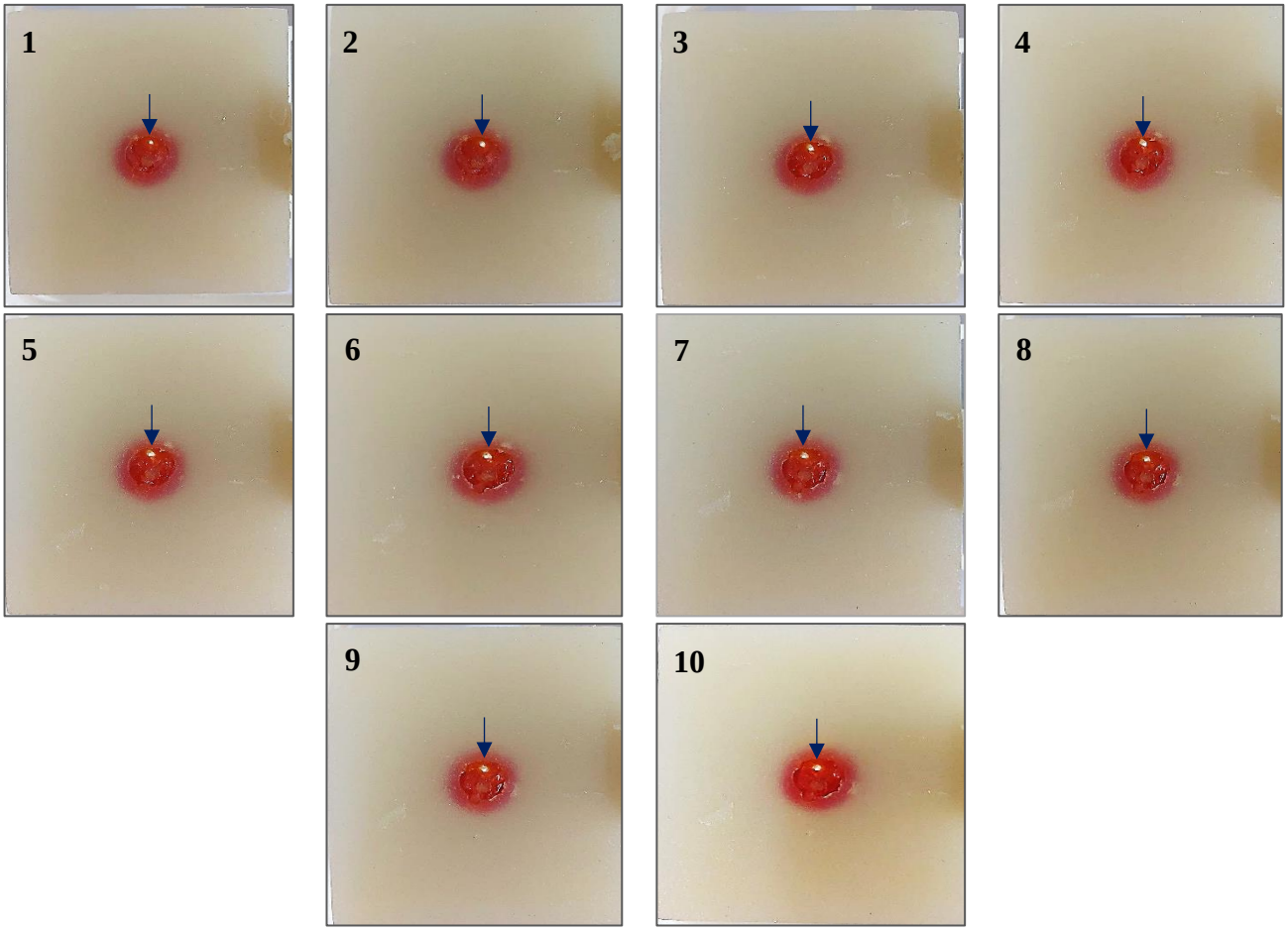

***Figure 5**: Needle tip location after motion execution and needle insertion in the cherry tomato for the 10 repetitions. Arrow indicates the plastic needle.*

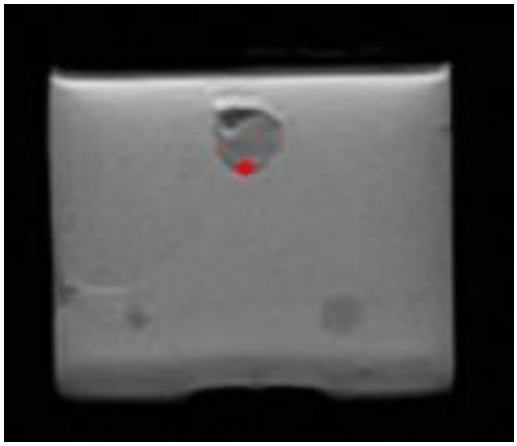

***Figure 6**: Target location as set on MRI image in the biopsy software (large tumour).*

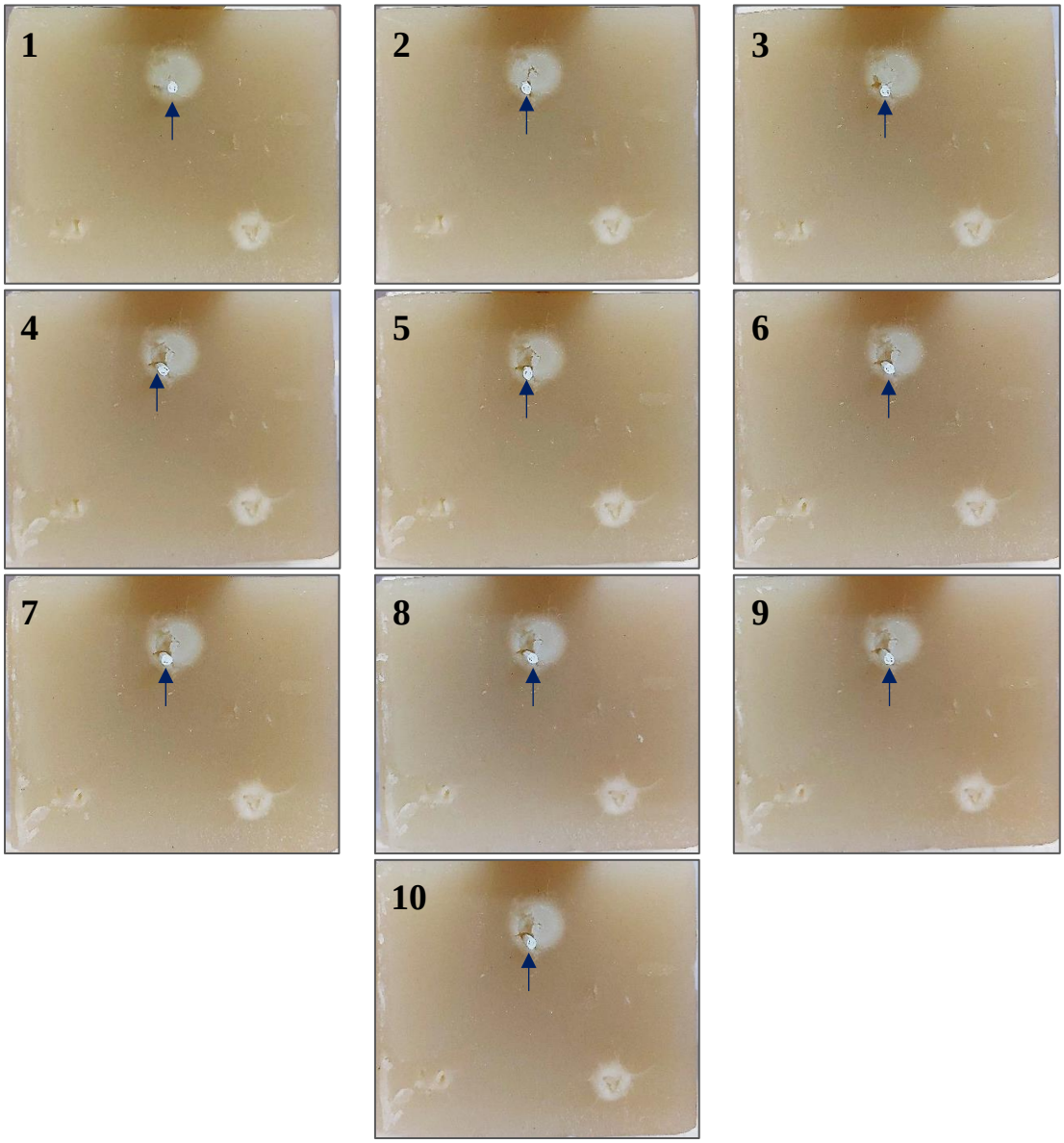

***Figure 7**: Needle tip location after motion execution and needle insertion in the large (15-mm diameter) tumour for the 10 repetitions. Arrow indicates the plastic needle.*

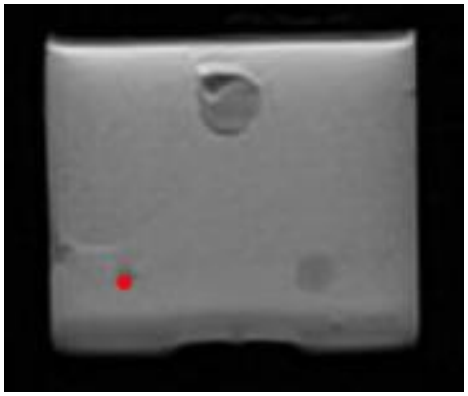

***Figure 8**: Target location as set on MRI image in the biopsy software (small tumour).*

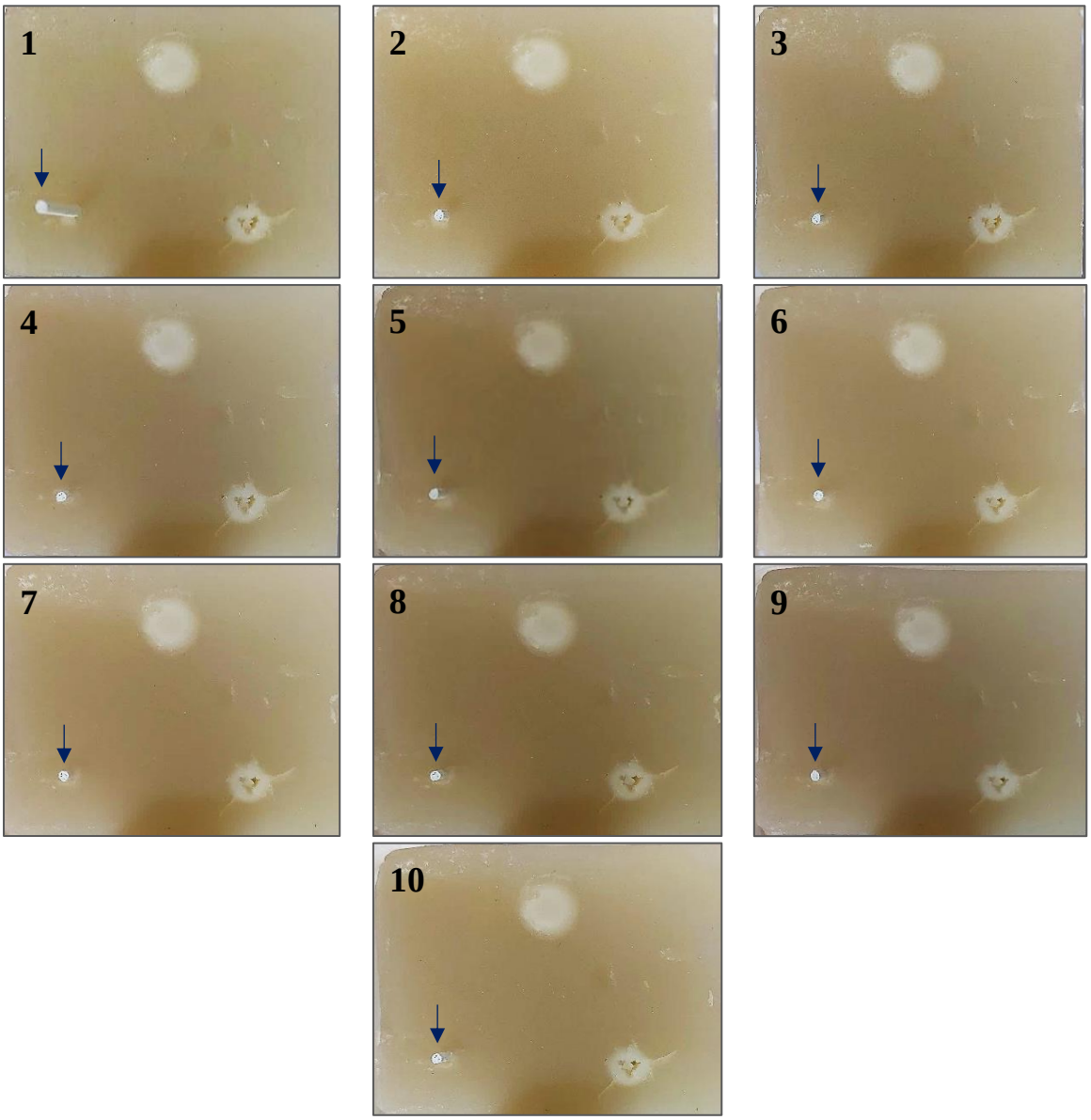

***Figure 9**: Needle tip location after motion execution and needle insertion in the small (5-mm diameter) tumour for the 10 repetitions. Arrow indicates the plastic needle.*

Laser-based method

Methodology

This experiment was carried out in another laboratory setting. The needle was replaced by a laser pointer (HY3003, Mastech DC Power Supply), which was navigated in the two PC-controlled axes (X and Y) to target preselected cells of the plastic grid shown in **Figure 10**. The cells had dimensions of 2 x 2 mm^2, and the thickness of the grid lines was 1 mm.

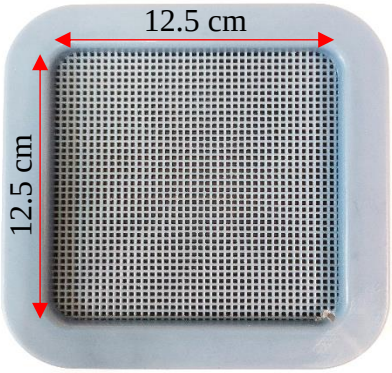

Figure 10*: Plastic grid utilized for assessing for the laser-based technique.*

Navigation planning for positioning the laser pointer to the desired location was based on MRI images as described in the previous section. Briefly, the user selected the desired cell on the relevant DICOM image of the grid, as shown in the software screenshot of **Figure 11**. The success of the procedure was determined by the location of the red light of the laser pointer, which was compared with the target position as set in the software. Overall, 20 grid cells were randomly selected and visited.

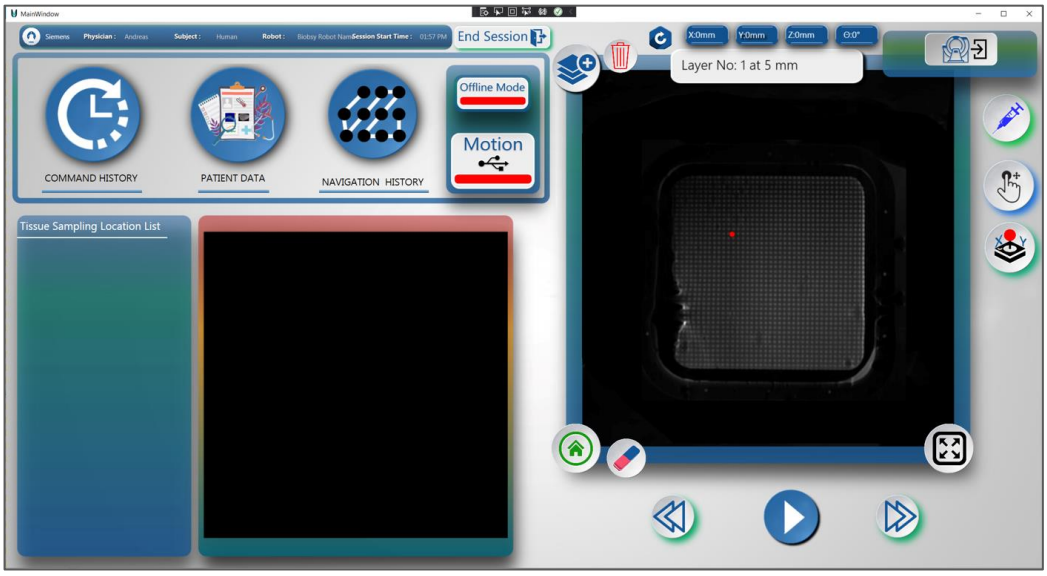

Figure 11*: Screenshot of the software during navigation planning.*

Results

Figure 12 shows indicative results for three targeted cells; one at the upper left, one in the center, and one at the lower right of the grid. The exact position of the red light was estimated by measuring the cells from the origin point in the X and Y axes and translating them to distance in mm. The results for all targeted cells are summarized in **Table 1**, which lists the actual and software coordinates for each visited cell. These results show a mean targeting error of 1.0 mm and 0.9 ± 0.3 mm in the X and Y axes, respectively.

Figure 12*: Column (A): Random grid cells selected on the software (3 different locations: No. 9, No. 17, No. 6 of Table 1). Column (B): The laser location after motion execution (3 different locations).*

Table 1: *List of the actual coordinates and software coordinates for each visited cell.*

	X (mm)		Y (mm)	
	Software	**Actual**	**Software**	**Actual**
1	65	66	56	57
2	68	69	53	54
3	38	39	74	75
4	86	87	89	90
5	47	48	77	78
6	38	39	50	51
7	62	63	71	72
8	50	51	80	81
9	**83**	**84**	**92**	**93**
10	50	51	54	54
11	56	57	83	84
12	89	90	50	51
13	44	45	74	75
14	32	33	57	57
15	53	54	80	81
16	29	30	80	81
17	**59**	**60**	**65**	**66**
18	50	51	83	84
19	86	87	77	78
20	65	66	47	48
Mean Difference (mm)	**1.0**		**0.9 ± 0.3**	

3. MRI evaluation

Methodology

Evaluation in a 1.5 T scanner

The targeting accuracy of the biopsy needle was then assessed by MRI. The experiment was carried out at the premises of the Germany Oncology Center (Limassol, Cyprus) in a 1.5 T scanner (GE Signa HD16, General Electric (GE), Chicago, Illinois, USA), in which an in-house made single-tumour phantom was utilized. The phantom was composed of an agar-based gel of 4 % weight per volume (w/v) agar (Merck KGaA, EMD Millipore Corporation, Darmstadt, Germany) mimicking breast tissue and an embedded tumour made of 6 % w/v agar, 4 % w/v silica (Sigma-Aldrich, St. Louis, Missouri, United States) and 30 % volume per volume (v/v) evaporated milk (Nounou, Friesland Campina, Marousi, Greece). The phantom can be seen in **Figure 13A**.

The robotic biopsy device was placed on the MRI couch with the phantom fixed on a specially designed holder, as shown in **Figure 13B**, and covered by a body coil (Signa 1.5T 12 Channel, GE Healthcare Coils, Aurora, Ohio, USA) with the assistance of a dedicated positioner, as shown in **Figure 13C**. The positioning mechanism was wired up to the electronic driving system located outside the MRI room through shielded cables.

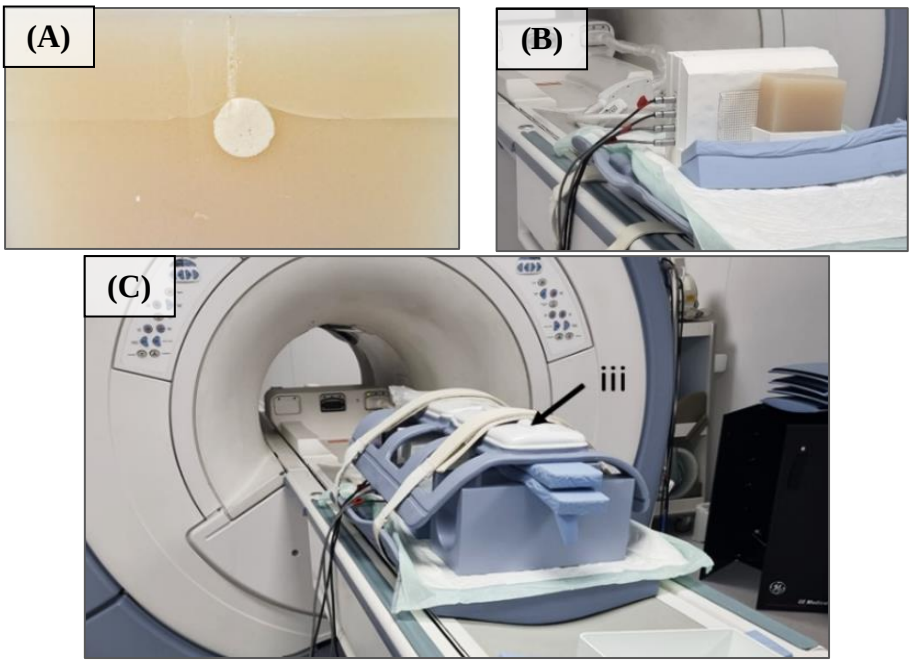

Figure 13*: Photos of the (A) single tumour phantom, (B) the robotic device seated on the MRI table with the phantom mounted on the holder, and (C) the experimental setup including the imaging coil.*

The biopsy needle was replaced by a syringe filled with water, which was navigated to reach the tumour in the phantom (in the X-Y plane) utilizing the navigation tools of the relevant biopsy software. Scans were acquired both at the level of the water-filled syringe and phantom, thus enabling registration of the syringe position relative to the targeted area as described in the relevant deliverable (D3.3). Image acquisition was performed utilizing a T1-weighted (T1-W) fast spin echo (FSE) sequence with the following parameters: Repetition time (TR) = 1000 ms, Echo time (TE) = 10.25 ms, Flip angle (FA) = 90º, ETL = 5, Pixel Bandwidth = 65.11 Hertz/pixel, Field of view (FOV) = 260 x 260 x 5 mm^3, matrix size = 224 x 192, No of averages (NEX) = 3, and acquisition time/slice = 122 s.

Evaluation in a 3 T scanner

Another experiment was carried out in a 3T MR scanner (MAGNETOM Vida, Siemens Healthineers, Erlangen, Germany). This study was carried out in the phantom containing a cherry tomato as the target, as well as in a phantom containing multiple biopsy targets. The agar-phantom (6% w/v) with the embedded cherry tomato is shown in **Figure 14A**. Note that it has a realistic breast-shaped design. The other one consisted of an agar gel of 6 % w/v agar and 2% w/v silicon dioxide mimicking breast tissue and embedded spherical tumour mimics made of 6% w/v agar and 6% w/v silica. The final phantom had a rectangular shape, a depth of 8 cm, and six embedded biopsy targets as shown in **Figure 14B**.

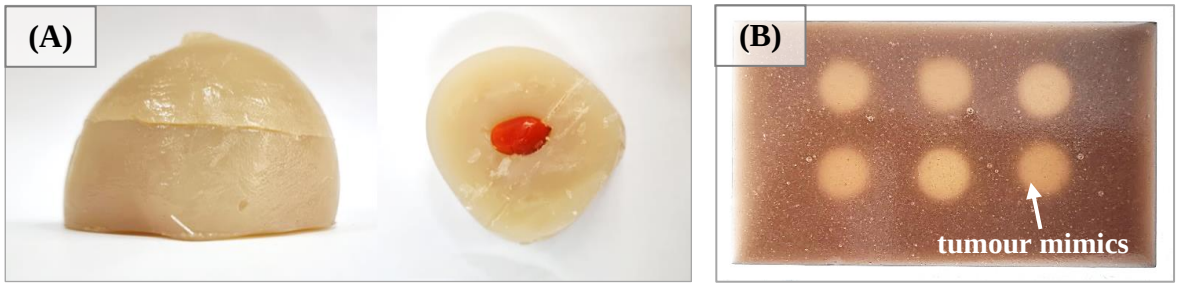

Figure 14: *Photos of the (A) Breast-shaped agar-based phantom (6 % w/v agar) featuring a cherry tomato: Isometric view (left) and Cross-section view (right), and (B) agar-based phantom with six biopsy targets.*

Specially designed 3D-printed holders were attached to the biopsy device for securely positioning the phantom in the robot's workspace, thus allowing direct insertion of the needle. The dedicated holder that accommodated the breast-shaped phantom can be seen in **Figure 15A**. The robotic biopsy device was securely placed on the MRI table, with a multi-channel body coil (18-channel, Siemens Healthineers, Erlangen, Germany) being properly fixed above the phantom using a dedicated plastic positioner, as shown in **Figure 15B**. Caution was given not to include the motors inside the coil detection area, thus reducing interference and SNR degradation.

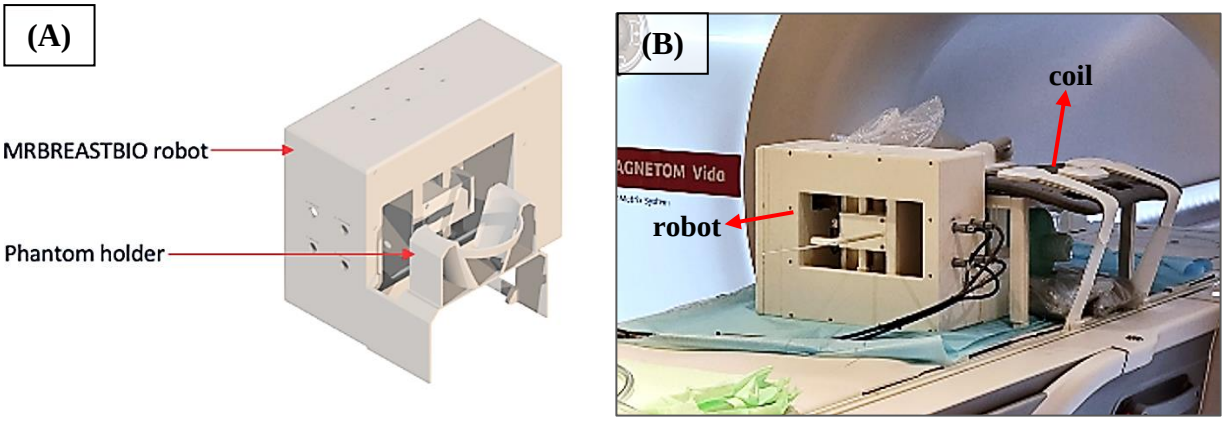

Figure 15: *A) CAD design of the MRBREASTBIO robot with a 3D-printed phantom holder attached. B) Experimental set-up inside the 3 T MRI scanner with the MRBREASTBIO robot placed on the table.*

A water-filled syringe was placed on the needle navigator of the robot. The breast-shaped agar-based phantom was positioned on the relevant holder, with an MR quality phantom placed next to it. **Figure 16** shows a 2D-Fast low angle shot (FLASH) localisation image acquired using the following parameters: TR = 7.8 ms, TE = 3.69 ms, FOV = 450×450 mm^2, Slice thickness = 6 mm, Matrix size = 256×205, NEX = 1, ETL = 1, Flip angle = 20^o, and Pixel Bandwidth = 320 Hz/pixel.

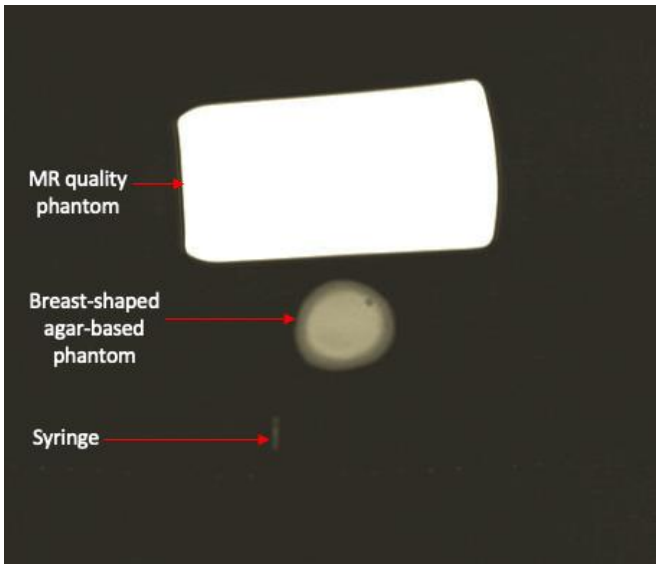

Figure 16: *Coronal localizer FLASH image of the experimental set-up showing the water-filled syringe as accommodated in the robot, the breast-shaped phantom as placed in the 3D-printed phantom holder and the MR quality phantom that was placed next to the set-up.*

Images of the syringe and the phantom were acquired, as shown in **Figure 17**, using a T2-W SE sequence with the following parameters: TR = 2000 ms, TE = 24 ms, FOV = 200×200 mm^2, Slice thickness = 10 mm, Matrix size = 128×128, NEX = 1, ETL = 16, Flip angle = 180^o, and Pixel Bandwidth = 200 Hz/pixel.

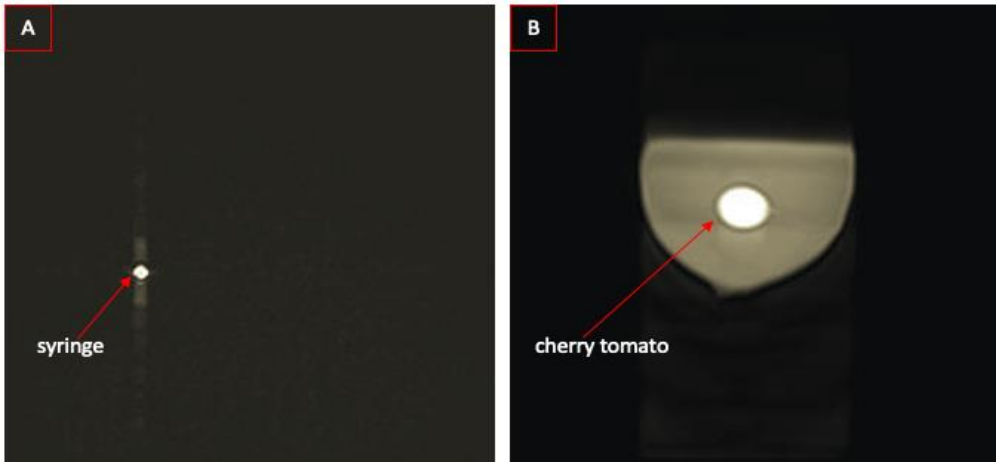

Figure 17*: Axial T2-W SE images showing A) the water-filled syringe as located at its initial position, and B) the breast-shaped agar-based (6 % w/v agar) phantom featuring a cherry tomato.*

Navigation planning for reaching the target (cherry tomato) was performed through the biopsy software using the acquired MR images. After robotic motion, T2-W images (with the abovementioned parameters) were acquired and fused to visualize the syringe position relative to the cherry tomato. The syringe was then replaced by a needle that was manually inserted in the target. Again, T2-W images were acquired for assessing the targeting accuracy.

For the multiple-tumour model, a similar localization approach was followed, and a specific tumour target was selected by the user through the software. The software then generated the corresponding location data and motion steps to be executed by the positioning mechanism, which were then transferred to the driving system to guide the needle to the desired location. After motion execution and manual needle insertion, image acquisition was performed with a T1-W Turbo Spin Echo (TSE) sequence with the following parameters: TR = 700 ms, TE = 23 ms, FA = 30°, ETL = 6, NEX = 2, Pixel bandwidth = 50 Hz/pixel, FOV = 280 x 280 x 10 mm^3, matrix size = 128 x 120, to detect the needle location relative to the targeted tumour mimic.

Results

Evaluation in a 1.5 T scanner

Figure 18 shows axial slices acquired using a T1-W FSE sequence at the location of the syringe and phantom, so that the syringe coordinates can be registered relative to the tumour coordinates. Accordingly, the MRI coordinates of the syringe and tumour are respectively indicated in **Figure 19A** and **Figure 19B**, whereas **Figure 19C** shows the new position of the syringe after motion execution, which coincides with the tumour's location (in X-Y plane).

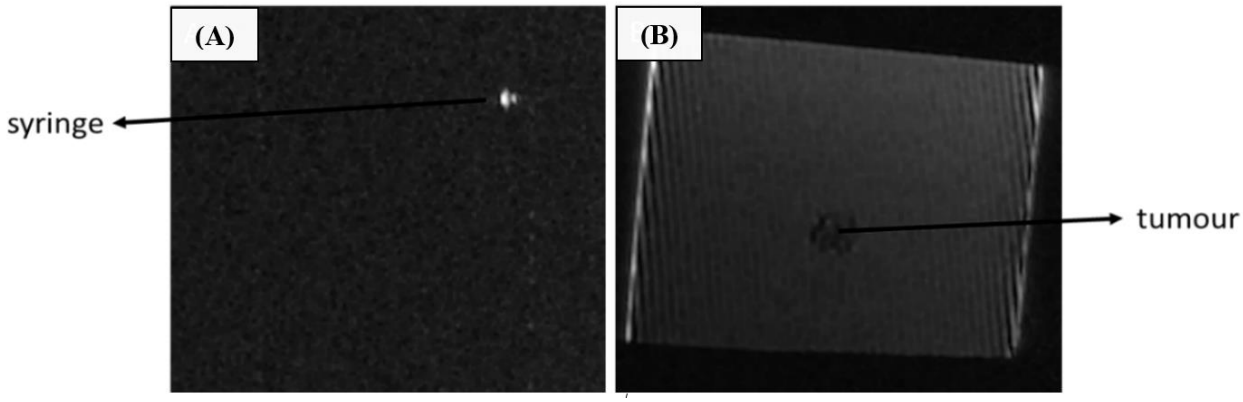

Figure 18*: Axial slices acquired using T1-W FSE sequence. (A) Slice positioned at the* syringe. *(B) Slice positioned at the tumour mimic in the phantom.*

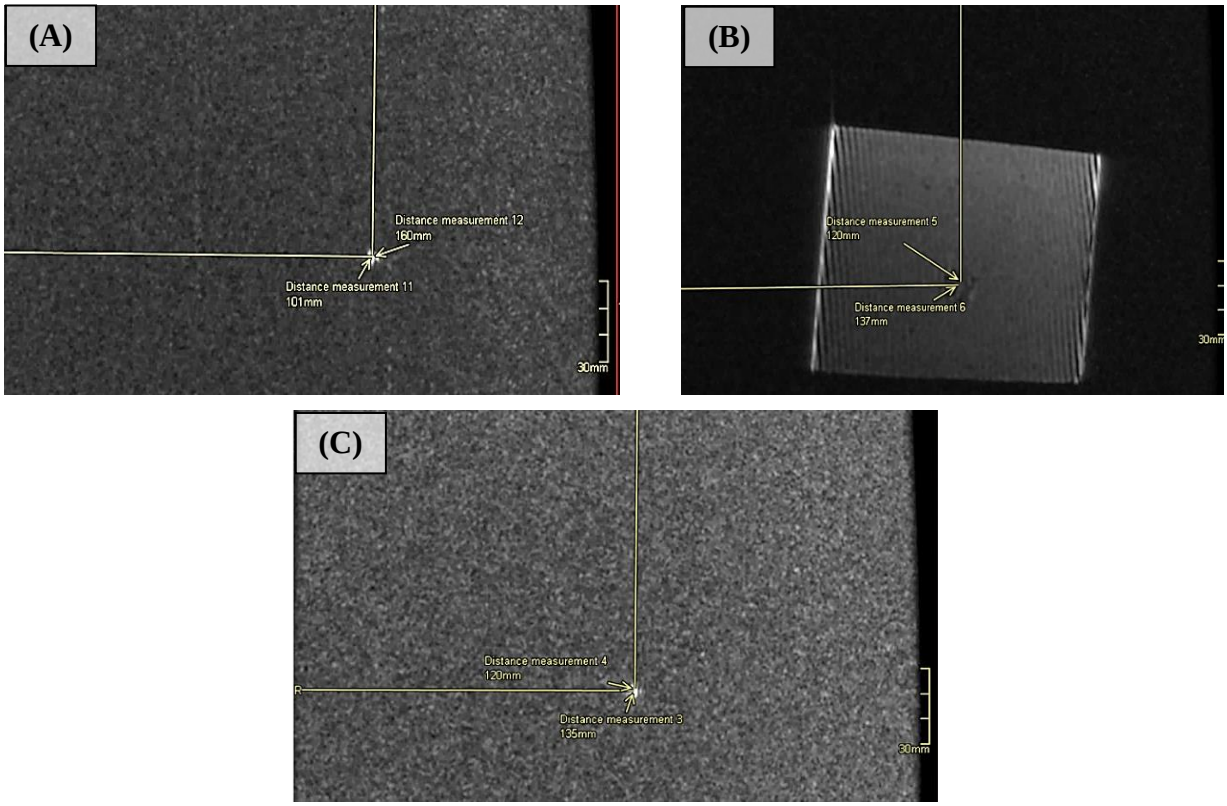

Figure 19*: (A) The position of the syringe before navigation. (B) The position of the lesion. (C) The position of the syringe after it was navigated to the tumour.*

Figure 20 shows fused T1-W FSE images where the two slices containing the syringe and phantom are overlapped. The fused images created before and after navigating the syringe to the tumour are compared. The dimensions of the syringe and tumour mimic as measured on the DICOM image are indicated in **Figure 21**. Finally, **Figure 22** presents a T1-W FSE image acquired in sagittal plane showing a needle inserted in the tumour mimic.

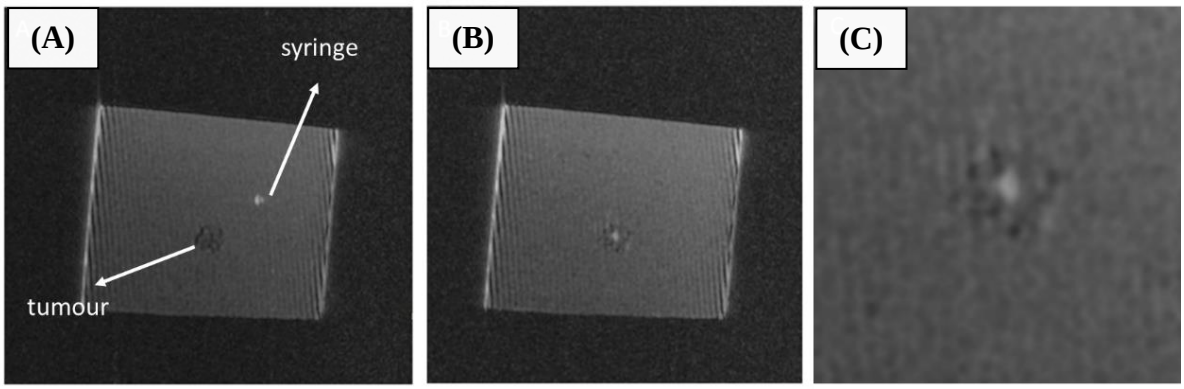

Figure 20*: Axial fused T1-W FSE images of the syringe and tumour (A) before navigation and (B) after navigation with the syringe targeting the tumour. (C) Enlarged image of the syringe targeting the tumour.*

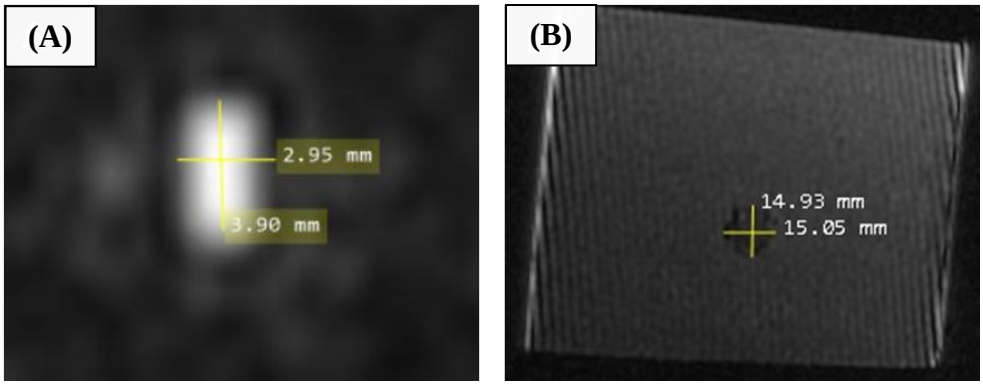

***Figure 21**: (A) Syringe and (B) tumour dimensions measured on the MRI image.*

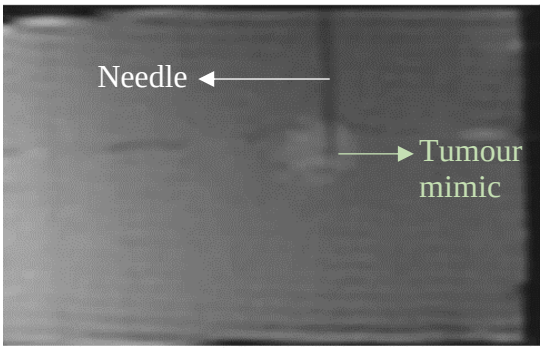

***Figure 22**: Sagittal image acquired using the T1-W FSE sequence showing the phantom with the needle inserted in the tumour mimic.*

Evaluation in a 3 T scanner

Indicative results of targeting accuracy obtained in the 3T MRI scanner are presented below. After localization and robotic motion based on navigation planning on pre-procedural MRI images, T2-W axial images at the level of the syringe and the cherry tomato were fused as shown in Figure 23A. Once confirming proper positioning of the syringe relative to the targeted tomato, the syringe was replaced by a needle that was manually inserted in the target. **Figure 23B** shows a T2-W image acquired after needle insertion, where the needle tip is visualized as a spot of reduced intensity within the tomato.

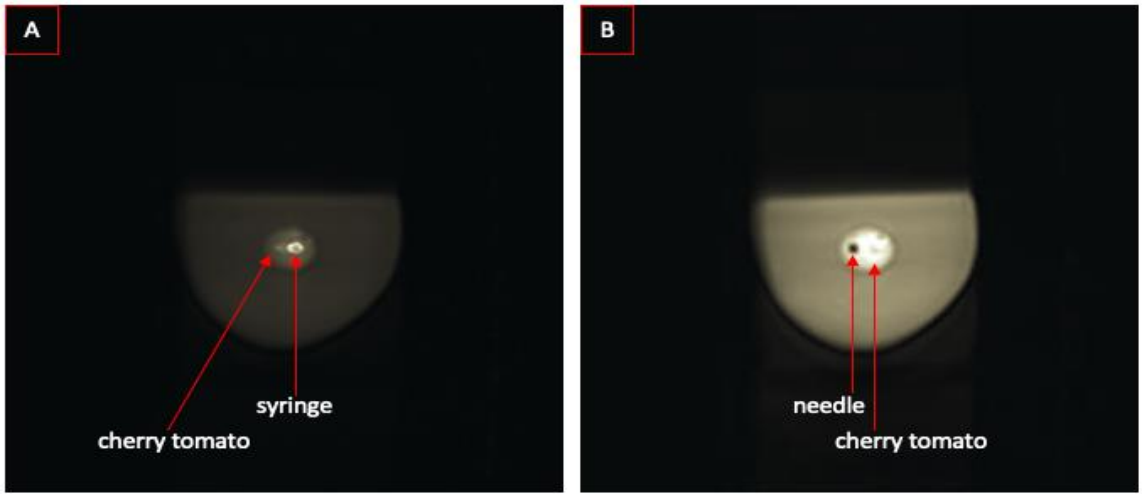

***Figure 23**: A) Fused axial T2-W SE images showing the location of the water-filled syringe relative to the cherry tomato. B) Axial T2-W SE image showing the needle as inserted in the cherry tomato.*

Figure 24 shows indicative results of the experiment carried out in the multiple-tumour phantom model, where the middle bottom tumour mimic was targeted. After motion execution, the needle tip was clearly visualized within the target in the T1-W image of **Figure 24A** without any significant susceptibility artifacts. **Figure 24B** is a photo of the punctured phantom.

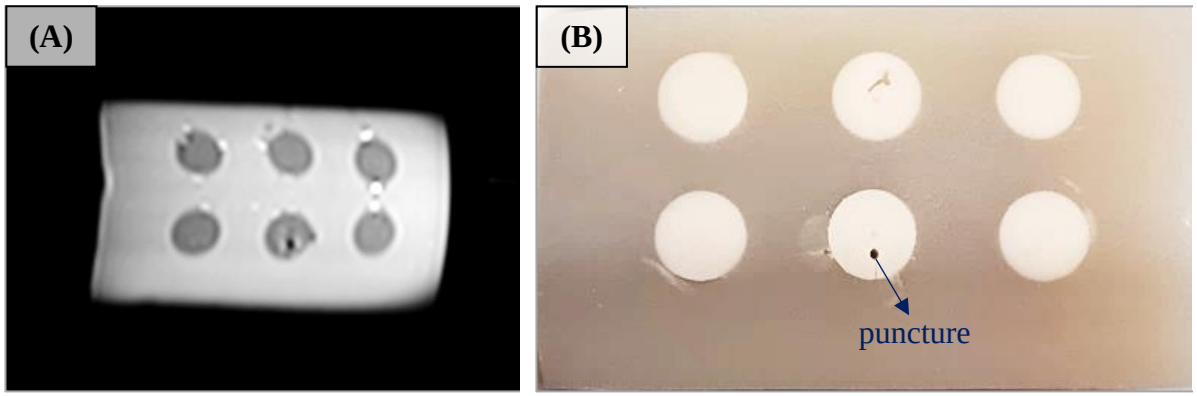

***Figure 24**: (A) T1-W image of the phantom after needle targeting. (B) Photo of the punctured phantom.*

4. Discussion

The current deliverable presented the results of the benchtop and MRI experiments carried out to assess the accuracy of the biopsy needle to reach the target. Agar based phantoms containing tumour mimics served as the main tool in this regard.

A repeatability test was carried out in the laboratory setting, where the needle was repetitively commanded (n=10) to reach phantom targets of different size (5-15 mm in diameter). After robotic positioning in a plane parallel to the grid, the needle was manually inserted in the phantom. The success of the procedure was assessed visually by checking whether the plastic needle pierced the tumour at the exact location defined by the software. In all the cases, the needle pierced the tumour successfully. Furthermore, excellent agreement in the location of the needle tip among repetitions was observed.

A laser-based approach was followed, where a laser pointer was navigated to target random cells of a plastic grid. In this case, the needle positioning error was defined by the difference in the location of the red light and the respective grid cell as selected in the software. A mean targeting error of 1.0 mm and 0.9 ± 0.3 mm was estimated for the X and Y axes, respectively.

Evaluation was also done in MRI scanners of 1.5 and 3 T field strength. The first technique involved the use of a water-filled syringe, which was navigated to reach a tumour mimic in the phantom. The syringe was navigated successfully without any software bugs and its new position coincided with the tumour's location as evidenced by fused SE images of the syringe and the phantom.

Once proper positioning of the needle navigator at the desired location as determined by the software coordinates (in the X-Y plane) was confirmed, the needle was manually inserted in the phantom to puncture the targeted tumour (along the Z-axis). The needle tip was clearly visualized within the tumour in follow up T1-W and T2-W images without noticeable susceptibility artifacts. Needle navigation relative to both a multiple-tumour phantom and an agar-based phantom containing a cherry tomato was performed successfully in the MRI setting.

Overall, the aforementioned results demonstrate high accuracy and repeatability of needle targeting, as well as proper functionality of the biopsy software and integrated navigation algorithms.

References

[1] K. G. Chan, T. Fielding, and M. Anvari, "An image-guided automated robot for MRI breast biopsy," *Int. J. Med. Robot. Comput. Assist. Surg.*, vol. 12, no. 3, pp. 461–477, 2016, doi: 10.1002/rcs.

[2] A. Patriciu, D. Petrisor, M. Muntener, D. Mazilu, M. Schär, and D. Stoianovici, "Automatic Brachytherapy Seed Placement Under MRI Guidance," *IEEE Trans Biomed Eng*, vol. 54, no. 8, pp. 1499–1506, 2007, doi: 10.1109/TBME.2007.900816.Automatic.

[3] N. Patel, J. Yan, R. Monfaredi, K. Sharma, K. Cleary, and I. Iordachita, "Preclinical evaluation of an integrated robotic system for magnetic resonance imaging guided shoulder arthrography," *Med. Imaging*, vol. 6, no. 2, 2019, doi: 10.1117/1.JMI.6.2.025006.

[4] H. Dou, S. Jiang, Z. Yang, L. Sun, X. Ma, and B. Huo, "Design and validation of a CT-guided robotic system for lung cancer brachytherapy:," *Med. Phys.*, vol. 44, no. 9, pp. 4828–4837, 2017, doi: 10.1002/mp.12435.

[5] M. A. Tavallaei, P. M. Johnson, J. Liu, and M. Drangova, "Design and evaluation of an MRI-compatible linear motion stage," *Med. Phys.*, vol. 43, no. 1, pp. 62–71, 2016, doi: 10.1118/1.4937780.

[6] Y. Koseki, T. Washio, K. Chinzei, and H. Iseki, "Endoscope Manipulator for Trans-nasal Neurosurgery, Optimized for and Compatible to Vertical Field Open MRI," *Med. Image Comput. Comput. Interv. — MICCAI 2002. MICCAI 2002. Lect. Notes Comput. Sci. Springer, Berlin, Heidelberg.*, vol. 2488, pp. 114–121, 2002.

[7] V. Groenhuis, F. J. Siepel, J. Veltman, J. K. van Zandwijk, and S. Stramigioli, "Stormram 4: An MR Safe Robotic System for Breast Biopsy," *Ann. Biomed. Eng.*, vol. 46, no. 10, pp. 1686–1696, 2018, doi: 10.1007/s10439-018-2051-5.

[8] "Ultrasound-Guided Breast Biopsy Phantom | Products: Patient Simulators for Diagnostic Training | Kyotokagaku Co., Ltd.," *Kyotokagaku.com*. [Online]. Available: https://www.kyotokagaku.com/products/detail01/us-9.html. [Accessed: 14-Jul-2020].

[9] "Stereotactic Needle Biopsy Phantom - CIRS," *CIRS*. [Online]. Available: https://www.cirsinc.com/products/mammography/stereotactic-needle-biopsy-phantom/. [Accessed: 14-Jul-2020].

[10] "Multi-Modality Breast Biopsy and Sonographic Trainer - CIRS," *CIRS*. [Online]. Available: https://www.cirsinc.com/products/ultrasound/zerdine-hydrogel/multi-modality-breast-biopsy-and-sonographic-trainer/. [Accessed: 14-Jul-2020].

[11] "Sun Nuclear Breast Biopsy Phantoms (Gammex™ Technology) - Sun Nuclear," *Sunnuclear.com*. [Online]. Available: https://www.sunnuclear.com/products/breast-biopsy-phantom-s. [Accessed: 14-Jul-2020].

[12] S. Y. Ng and C. Lin, "Low-cost and easily fabricated ultrasound-guided breast phantom for breast biopsy training," *Prepr. (Version 1) available Res. Sq.*, pp. 1–22, 2020, doi: 10.21203/rs.2.19957/v1.

[13] A. Fenster, K. J. M. Surry, G. R. Mills, and D. B. Downney, "3D ultrasound guided breast biopsy system," *Ultrasonics*, vol. 42, pp. 769–774, 2004, doi: 10.1016/j.ultras.2003.11.004.

[14] R. Werner *et al.*, "MR-Guided Breast Biopsy Using an Active Marker : A Phantom Study," *J. Magn. Reson. Imaging*, vol. 24, pp. 235–241, 2006, doi: 10.1002/jmri.20600.

[15] E. Schneider, K. W. Rohling, M. D. Schnall, R. O. Giaquinto, E. A. Morris, and D. Ballon, "An Apparatus for MR-Guided Breast Lesion Localization and Core Biopsy : Design and Preliminary Results," *J. Magn. Reson. Imaging*, vol. 14, pp. 243–253, 2001, doi: 10.1002/jmri.1180.

[16] B. L. Daniel *et al.*, "An MRI-Compatible Semiautomated VacuumAssisted Breast Biopsy System: Initial Feasibility Study," *J. Magn. Reson. Imaging*, vol. 644, pp. 637–

644, 2005, doi: 10.1002/jmri.20302.
[17] B. L. Daniel, R. L. Birdwell, J. W. Black, D. M. Ikeda, G. H. Glover, and R. J. Herfkens, “Interactive MR-guided, 14-gauge core-needle biopsy of enhancing lesions in a breast phantom model,” *Acad. Radiol.*, vol. 4, no. 7, pp. 508–512, 1997, doi: 10.1016/S1076-6332(97)80238-3.